Quantitative Absorption Measurements Using Cavity-Ringdown Spectroscopy with Pulsed Lasers

J. Patrick Looney, Joseph T. Hodges, and Roger D. van Zee

Chemistry Science and Technology Laboratory, National Institute of Standards and Technology, Gaithersburg, MD 20899

The theory and implementation of quantitative gas phase absorption measurements based on cavity-ringdown spectroscopy with pulsed lasers is discussed. The response of ringdown cavities is modeled using an eigenmode description of the cavity fields, and expressions for a number of measurable quantities are given in terms of experimental parameters. Results for long and short ringdown cavities are presented and compared, and it is shown that absolute, high-resolution absorption line shapes can be obtained using a pulsed laser and a short cavity.

Cavity-ringdown spectroscopy (CRDS) is a relatively new absorption spectroscopy that promises sensitive and accurate absorption measurements. The power of CRDS for trace gas monitoring and quantitative absorption measurements was recognized from the earliest measurements by O'Keefe and Deacon *(1)*. Absorptivity measurements of $<10^{-9}$ cm^{-1} have been reported *(2)*, and the shot-noise detection limit is $<10^{-13}$ cm^{-1}.

A conventional implementation *(3)* of CRDS uses a pulsed laser to excite a linear cavity formed from two highly reflective, spherical mirrors. Usually the cavity design is not particularly special, (*i.e.* not confocal or otherwise degenerate), and the cavity is not length stabilized. In such an arrangement, a cavity can store the optical field for durations as long as 10^{-4} s, during which time the intensity decays exponentially in time with a time constant called the ringdown time. This decay is measured at the exit of the cavity, the signal is digitized, and the ringdown time is extracted from the digitized signal. For a cavity filled with an absorbing gas under conditions when the Beer-Lambert law is valid, the ring-down time is extracted using the relationship,

$$\tau(\omega) = \frac{\ell}{c \cdot [(1-R) + \alpha(\omega)\ell]}, \qquad (1)$$

where ℓ is the cavity length, R is the intensity reflectivity of the mirror, $\alpha(\omega)$ is the frequency dependent absorption coefficient, and c is the speed of light.

Making measurements with the best sensitivity and the highest accuracy is one objective of our ongoing research. In this chapter, we explore how such measurements can best be made. Below, we review the theoretical underpinning of the method, provide predictive formulae for some of the observable signals, and discuss alternative measurement strategies and present corresponding data.

Theoretical Model of Cavity-Ringdown Spectroscopy.

This section discusses the theory behind ringdown signals using a field-based description of ringdown signals. Detailed derivations for the starting formulae used below have been given before *(4,5)* and are not repeated here. Expressions for the signal as a function of time, the peak power levels, the transmitted energy, and ultimate detection limits are derived below.

Field-based Derivation of Cavity-Ringdown Signals. The response of a ringdown cavity to the incident excitation field is embodied by the eigenmodes of the cavity *(4-7)*. The net field exiting a ringdown cavity is simply a weighted sum of all of the excited cavity eigenmodes, where the weighting of each mode depends on the overlap of the excitation field spectrum with the cavity eigenfrequency structure, and on the spatial overlap of the transverse profile of the incident field with the spatial structure of the cavity eigenmodes. The overall measured signal is proportional to the modulus squared of the total field exiting the cavity.

The Excitation Field. For a transform-limited, Gaussian pulse centered at frequency ω_c, the input field to the cavity can be written as

$$\tilde{E}_i(x,y,z,\omega) = \tilde{e}_i(\omega)u_i(x,y,z) = E_0 \frac{\sqrt{\pi}}{\sigma_\omega} e^{-(\omega-\omega_c)^2/4\sigma_\omega^2} u_i(x,y,z). \qquad (2)$$

In this expression, $u_i(x,y,z)$ specifies the transverse profile of the incident field along the z axis, and $\tilde{e}_i(\omega)$ the spectrum of the field. The spectral width of this incident field, σ_ω, is related to the temporal duration of the pulse, σ_t, through the relation $\sigma_\omega = (2\sigma_t)^{-1}$. Of course, the width of the associated power spectrum is $2^{-1/2}$ as wide as the field spectrum, since it is proportional to the square of the field spectrum.

The Cavity. The ringdown cavity discussed here is a Fabry-Pérot resonator, and its eigenfrequency structure is a series of narrow resonances, each centered at a cavity eigenfrequency. The spacing of the cavity eigenfrequencies is determined from the geometry of the cavity and the index of the medium filling the cavity. For a symmetric cavity formed from two reflectors with radius of curvature, r, and separated by a length, ℓ, such that $\ell < 2r$ and filled with a medium with index of refraction $n(\omega)$, the resonance frequencies are given by *(8)*

$$\nu_{qmn} = \frac{\omega_{qmn}}{2\pi} = \frac{c}{2\cdot\ell\cdot n(\omega_{qmn})}\left\{ q + \frac{1}{\pi}(m+n+1)\cos^{-1}[1-(\ell/r)]\right\}. \qquad (3)$$

The three indices $\{q,m,n\}$ uniquely label each mode. The index q designates the longitudinal mode and the indices $\{m,n\}$ the transverse mode. Only cavities of specific lengths are degenerate, that is, have a transverse mode spacing [Δq=0, $\Delta(m+n)$ =1] that is a rationally related ratio of the longitudinal mode spacing [Δq=1, $\Delta(m+n)$ =0] which is also referred to as the free spectral range, $\Delta\omega_f$. For nondegenerate cavities, there can be a mode at essentially any arbitrary frequency, though the transverse mode indices may be large.

When a Fabry-Pérot resonator is irradiated, only certain components of the incident field spectrum are efficiently transmitted. The ratio of the transmitted field to the incident field is described by a frequency dependent function referred to as the cavity response function. This function is commonly known as Airy's formula when the cavity is empty *(9)*. When the mirror reflectivities are near unity, as it is for a ringdown cavity, Airy's formula can be approximated as a superposition of isolated Lorentzians centered at the cavity resonances or eigenfrequencies. This structure simply reflects the fact that only light centered at the cavity eigenfrequencies can resonate within the cavity because of the boundary conditions imposed by the mirrors *(5)*.

If the cavity is filled with an absorber, two things happen to the cavity response function. First, the resonance frequencies are shifted, though by such small amounts that these shifts are ignored here. Second, each of the resonances in the vicinity of a spectral absorption feature is broadened and its peak is decreased. In the limit of Beer-Lambert law absorption, the cavity response function associated with mode $\{q,m,n\}$ is given by

$$\tilde{\mathcal{H}}_{qmn}(\omega) \approx \left[\frac{1-R}{1-Re^{-\alpha(\omega)\ell}}\right]\frac{\Gamma_{qmn}e^{-\alpha(\omega)\ell/2}}{(\Gamma_{qmn} - i(\omega-\omega_{qmn}))} \qquad (4)$$

where the mode width is given by

$$\Gamma_{qmn} = \frac{1}{2\tau_{qmn}} = \frac{1-Re^{-\alpha(\omega_{qmn})\ell}}{t_r} \equiv \frac{T_{eff}(\omega_{qmn})}{t_r} \qquad (5)$$

and where T_{eff} is an effective single pass intensity transmittance and τ_{qmn} is the intensity ringdown time for the specified mode. Note that in the limit, $\alpha(\omega)\to 0$ and for the specified resonance, Equation 4 reduces to the Lorentzian approximation of Airy's formula *(5)*.

The Cavity Excitation. For pulsed excitation, the frequency spectrum of the excitation field is composed of many frequencies. As discussed above, the field spectrum of mode $\{q,m,n\}$ exiting the cavity $\tilde{e}_{qmn}(\omega)$ is the product of the cavity response function and the incident field spectrum,

$$\tilde{e}_{qmn}(\omega) = \tilde{\mathcal{H}}_{qmn}(\omega)\ \tilde{e}_i(\omega)\ . \qquad (6)$$

The number of cavity modes excited depends upon the spacing of these cavity modes relative to the bandwidth of the excitation laser. It is useful then to define a characteristic dimensionless parameter, $\eta = 2\sigma_\omega/\omega_f$. A pictorial representation of the

cavity excitation in the frequency domain is given in Figure 1. The cavity response function is plotted versus frequency. Superimposed on this figure is the excitation spectrum of the incident laser field. As the cavity resonances are quite narrow, they appear as spikes. The two cases depicted in this figure correspond to a cavity mode spacing that is much larger than the excitation bandwidth, or $\eta << 1$ (Figure 1a) and to a mode spacing that is small compared to the laser bandwidth, or $\eta > 1$ (Figure 1c). These two cases are designated as the short- and long-cavity limits, respectively. In the long-cavity limit, η represents the number of cavity modes that is excited.

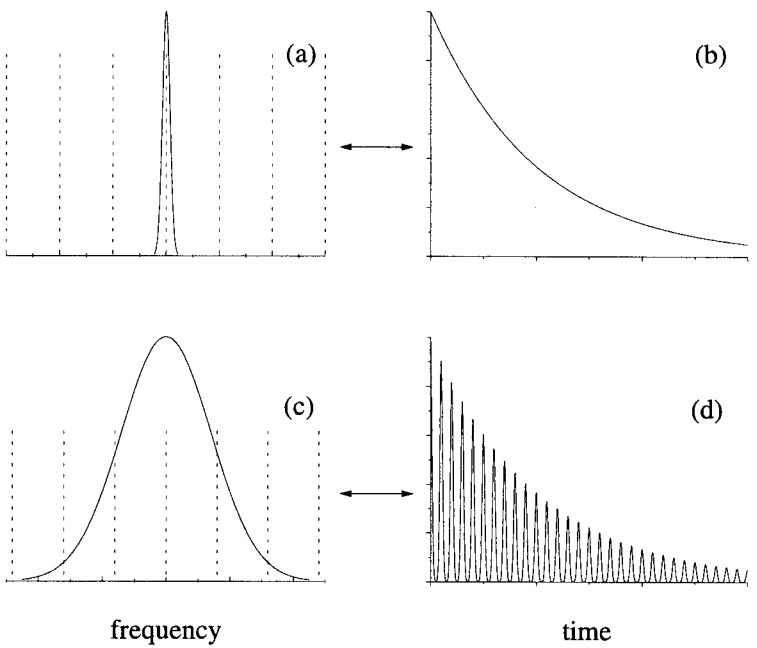

Figure 1: This figure illustrates excitation of a ringdown cavity by a transform-limited, Gaussian pulse. On the left, the longitudinal mode structure and excitation field spectrum are shown for a short (a) and a long (c) ringdown cavity. On the right, the corresponding ringdown signals are shown.

The excitation of cavity modes also depends upon the spatial coupling of the light into the cavity. The spatial overlap factor C_{mn} is given by the projection of the incident field, $u_i(x,y,z)$, onto the transverse mode functions of the cavity *(4,5)*,

$$C_{mn} = \int_{-\infty}^{\infty}\int_{-\infty}^{\infty} u_i(x,y,-\ell/2)\ \psi^*_{mn}(x,y,-\ell/2)\ dxdy\,. \qquad (7)$$

Here, $\psi_{mn}(x,y,z)$ are the Gauss-Hermite polynomials. The spatial partitioning of the laser input energy among the different cavity transverse modes is given by $f_{mn} = |C_{mn}|^2/\Sigma|C_{mn}|^2$.

For perfect mode matching into a single transverse mode there is only one non-zero f_{mn} which, in this case, must be unity. Multiple transverse modes may be excited if the incident wavefront is not matched to a single cavity mode. It is worth noting that the intensity coupling is proportional to the square of these coefficients. In practice, good mode matching is not readily achieved without spatial filtering of the input beam, a judicious choice of the coupling optics, careful alignment of the cavity, and monitoring of the transverse profile of the light exiting the cavity.

CRDS Signals. The net field exiting the cavity at frequency ω is simply the weighted sum of all of the excited eigenmodes of the cavity. This is given by *(5)*

$$\tilde{E}(x,y,\ell/2,\omega) = \sum_{q}\sum_{mn} C_{mn}\psi_{mn}(x,y,\ell/2)\ \tilde{e}_{qmn}(\omega)\ . \tag{8}$$

Fourier transformation yields the time evolution. Spatial integration of the resulting intensity then yields the radiant power, which is the quantity measured in the laboratory.

For the excitation field described in Equation 4 with a pulse energy $\mathscr{E}_p$, the total power radiated from a given excited transverse mode as measured at the exit of the cavity is *(5)*

$$\dot{\mathscr{E}}_{mn}(t) = \sqrt{2\pi}\ \mathscr{E}_p\left[\frac{T^2}{\sigma_\omega t_r^2}\right] f_{mn}\left\{\sum_{q=1}^{\infty} e^{-\alpha(\omega_{qmn})\ell}\ e^{-(\omega_{qmn}-\omega_c)^2/2\sigma_\omega^2}\cdot e^{-2\Gamma_{qmn}t}\right.$$

$$+\ 2\sum_{q=1}^{\infty}\sum_{q'=q+1}^{\infty} e^{-\alpha(\omega_{q'mn})\ell/2}\ e^{-\alpha(\omega_{qmn})\ell/2}\ e^{-(\omega_{qmn}-\omega_c)^2/4\sigma_\omega^2}\ e^{-(\omega_{q'mn}-\omega_c)^2/4\sigma_\omega^2}\cdot \tag{9}$$

$$\left. e^{-(\Gamma_{qmn}+\Gamma_{q'mn})t}\cdot\cos[(\omega_{qmn}-\omega_{q'mn})t]\right\}\ .$$

This expression is in general valid for times that are larger than the laser's pulse duration. The single summation describes the envelope of the ringdown signal and is the weighted sum of exponential decays from the excitation of multiple longitudinal modes. Each term in this sum has a decay time based on the optical losses in the cavity at the corresponding eigenfrequency, with each weighting factor being dependent upon the spectral overlap of the excitation spectrum with the cavity eigenfrequency. If the line widths of the excited modes are constant with mode index, which is to say all modes have the same losses, then the envelope of the decay will be purely exponential. The double summation in Equation 9 contains the interference terms arising from the beating of different excited longitudinal modes. These exponentially decaying terms sinusoidally modulate the envelope signal. Since the mode-beating terms contain negligible energy, the net transmitted energy is essentially all contained within the envelope of the decay given by the single summation in Equation 9. If more than one transverse mode of the cavity is excited, then the total measured signal is the sum over all of the excited transverse modes. Transverse mode beating can give rise to additional complexities *(4,5)*.

Assuming the excitation of a single transverse mode, in the short-cavity limit only one longitudinal mode contributes to the total signal and the optical decay is a simple

exponential decay (Figure 1b). In the long-cavity limit, many longitudinal modes contribute to the signal and the observed optical decay signal is a series of "pulses" of decaying amplitude, each separated by the round-trip time in the cavity (Figure 1d). In the intermediate cavity case, a few cavity modes are excited and the observed decays will show modulations with the depth of modulation dependent on ω_c. If the dispersion within the cavity cannot be neglected, then the cavity eigenmodes will no longer be equally spaced and the mode-beating will no longer be strictly periodic *(4)*. This effect, in turn, will alter the shape of the pulses leaving the cavity.

Signal Power Levels and the Energy Transmitted by the Cavity. Evaluated at t=0, the single summation in Equation 9 gives the peak power radiated by a single cavity mode. The total transmitted energy is determined by integrating Equation 9 over all time. Table I gives expressions for these quantities in the long- and short-cavity cases and summarizes some of the other properties of ringdown cavities that have been discussed above. It is interesting to note that the peak power levels in the cavity at the end mirror will be a factor of $\sqrt{2/\pi\eta^2}$ greater in the short-cavity limit when compared to the peak power for the long cavity excited by the same pulse. For incident pulse energies of ~1 mJ, the intra-cavity power levels for a short cavity can be sufficient to make absorption rates exceed relaxation and dephasing rates for strong transitions. This may lead to saturation phenomena such as hole burning *(10)* and to non-exponential ringdown signals. Coupled with the very high spectral resolution of single-cavity mode spectroscopy, this regime may provide an area of future interest in CRDS measurements.

Statistical Uncertainties in CRDS-based Absorption Measurements.

Since absorption measurements in CRDS are made by measuring on-resonance losses and subtracting the empty cavity losses, the overall uncertainty in the absorption coefficient depends upon the uncertainty in the mean ringdown time of both the on- and off-resonance measurements. Therefore, the minimum measurable absorption coefficient for many independent measurements is *(2)*

$$\alpha_{\min} = \sqrt{2}\,\frac{\sigma_{\tau_{empty}} / \bar{\tau}_{empty}}{c\,\bar{\tau}_{empty}}\,, \qquad (10)$$

where $\sigma_{\tau_{empty}}$ is the uncertainty (typically expressed as a standard deviation) in the mean value of the empty cavity ringdown time $\bar{\tau}_{empty}$. In the shot noise limit, the ratio $\sigma_{\tau_{empty}} / \bar{\tau}_{empty}$ is the reciprocal of the square root of the number of detected photons. However, in practice, this ratio is determined by an appropriate statistical analysis of the ensemble of time constant measurements, and this measured value may very well be larger than the shot-noise limited value. In Table I, expressions for α_{min} are given for the long- and short-cavity cases assuming shot-noise limited detection. Shot-noise limited values of α_{min} range from 10^{-9} - 10^{-13} cm^{-1} for realistic parameters. The midpoint of these absorptivity limits corresponds to number densities of ~10^{16} m^{-3} in the case of a very weak absorption band, such as the b(v=0) ← X(v=0) electronic transitions of molecular oxygen or ~10^{11} m^{-3} for a strong absorber, such as the (00011) ← (00001) vibrational band of carbon dioxide.

Table I. Comparison of Short and Long Cavity Properties to Pulsed Gaussian Excitation.

	Short ($\eta << 1$)	*Long* ($\eta > 1$)
Signal	Single Exponential Decay	Series of Recurring "Pulses"
Peak Power in Ring-Down Signal (*e.g.* Watts)	$\mathscr{E}_p \dfrac{\sqrt{2\pi}\, T^2}{\sigma_\omega t_r^2} f_{mn}\, e^{-(\omega_{qmn}-\omega_c)^2/2\sigma_\omega^2}$	$\mathscr{E}_p \dfrac{T^2}{t_r} f_{mn}$
Energy Transmitted (*e.g.* Joules)	$\mathscr{E}_p \dfrac{\sqrt{\pi/2}\, T^2}{\sigma_\omega t_r^2 \Gamma_{qmn}} f_{mn}\, e^{-(\omega_{qmn}-\omega_c)^2/2\sigma_\omega^2}$	$\mathscr{E}_p \dfrac{\sqrt{\pi/2}\, T^2}{\sigma_\omega t_r} f_{mn} \sum_{q=1}^{\infty} \dfrac{e^{-(\omega_{qmn}-\omega_c)^2/2\sigma_\omega^2}}{1-Re^{-\alpha(\omega_{qmn}-\omega_0)\ell}}$ ‡
Shot-Noise Limited Absorptivity (α_{min}) (*e.g.* cm^{-1})	$\dfrac{2}{\ell}\sqrt{\dfrac{h\nu}{\mathscr{E}_p\beta}\dfrac{\eta}{\sqrt{2/\pi}}\dfrac{T}{N_s}}$	$\dfrac{2}{\ell}\sqrt{\dfrac{h\nu}{\mathscr{E}_p\beta}\dfrac{T}{N_s}}$

η	$= 2\sigma_\omega / \Delta\omega_f$	= ratio of excitation spectral linewidth to cavity free spectral range.
σ_ω		$= e^{-1/2}$ width of power spectrum of incident laser pulse.
$\Delta\omega_f$	$= \pi c / \ell$	= cavity free spectral range (c = speed of light, ℓ = cavity length).
$\omega_{qmn} - \omega_c$		= detuning of mode $\{q,m,n\}$ from laser central frequency.
$\omega_{qmn} - \omega_0$		= detuning of mode $\{q,m,n\}$ from absorption line center.
f_{mn}		= fraction of incident light coupled into the $\{m,n\}$ transverse mode.
t_r	$= 2\ell / c$	= cavity round-trip time.
T	$= 1 - R$	= intensity transmittance of cavity mirrors (R = intensity reflectivity).
Γ_{qmn}	$= (2 * \tau_{qmn})^{-1}$	= linewidth of cavity mode $\{q,m,n\}$ (τ_{qmn} = ringdown time).

$\mathscr{E}_p$	= incident laser pulse energy.
$h\nu$	= photon energy.
β	= dectector quantum efficiency.
N_s	= number of shots.
‡	= reduces to $\mathscr{E}_p f_{mn}\, T/2$ for an empty cavity.

The best estimation of the ringdown time is determined from a weighted, least-squares regression to the natural logarithm of the ringdown signal *(11)*. Our current approach is to identify the dominant noise sources and estimate noise levels to obtain the weighting factors. To account for baseline effects, the average value of the digitized baseline signal that precedes each exponential decay is determined, and this level is subtracted from the ringdown signal. The time constant is then simply the reciprocal of the best-fit slope.

The weighting factors are equal to the reciprocal of the overall signal variance. The signal variance due to shot noise can be estimated in terms of the measured signal level, detector responsivity, and the system bandwidth. The digitizer noise is based on the vertical resolution of the oscilloscope, and the detector's technical noise is given by the measured variance in the baseline signal. All three variances are summed to give the total variance. When the data are weighted in this manner, the ringdown signals have a reduced-χ^2 near unity, indicating a good fit *(11)*. In fact, the reduced-χ^2 was found to be a very sensitive measure of the quality of our ringdown curves.

Quantitative Absorption Measurements.

Above, the shape of ringdown signals was considered in the long- and short-cavity limits. It was seen that in the long-cavity limit, a ringdown signal consists of a series of decaying "pulses" that result from beating between the longitudinal modes that are excited by the incident light. If longitudinal modes with different transverse indices (m and n) are excited, and if, as is typical in real experiments, complete orthogonality between the transverse modes cannot be maintained, then additional mode beats will occur *(4,5)*. This transverse mode beating only further complicates the observed signals. Consequently, the accuracy of absorptivity measurements determined from such ringdown curves can be expected to be compromised because of the difficulty associated in extracting the decay constant from complex signals. Furthermore, even if only a single transverse mode is excited (perfect mode matching), under certain circumstances the ringdown signal will not be purely exponential. Specifically, for a long cavity and if the line width of the absorbing feature is comparable to the spectral width of the incident light, the overall decay will actually be a superposition of many exponentials. Thus, as predicted by Equations 5 & 9, the signal comprises multiple modes each decaying at a different rate. For this case, some type of backcorrection to the signals will be required to obtain $\alpha(\omega)$ *(6)*.

In the limit of a short cavity, on the other hand, a single mode excitation can be more simply realized. Thus, to the extent that a single transverse mode is dominant, the ringdown signals can be expected to be single exponentials. Because each mode of a ringdown cavity is extremely narrow, the absorptivity over an essentially infinitesimal frequency interval is measured, so that no backcorrection is required. It would therefore be expected that the most accurate absorptivity measurements could be made in this short- cavity limit.

Below, data are presented for both a conventional, long-cavity and short-cavity implementation of CRDS.

Conventional CRDS Measurements. To investigate the accuracy of the ringdown technique, we have previously reported CRDS measurements of Doppler-broadened transitions of the b(v=0) ← X(v=0) band of $^{16}O_2$ using a conventional CRDS setup *(12)*. The cavity was 1.2 m long and nondegenerate, and was excited by a single-mode Ti:Al_2O_3 laser with an effective spectral bandwidth of ~250 MHz. Based on the single-shot laser bandwidth, η~1.0 for this experiment. Neither the length of the ringdown cavity nor the laser frequency was stabilized, and multiple transverse modes were intentionally excited by off-axis injection of the laser *(4,5,13)*. Multiple ringdown signals were averaged, and the time averaged spectrum of the laser was simultaneously recorded. The electronic bandwidth of the detection system was 30 MHz. Data obtained on resonance were modeled using the integral formulation (Equation 1 of Reference 12) for the decay signals to extract the line strengths of the rotational transitions.

To illustrate the results, we show in Figure 2a a 25-shot average of the optical decay measured on the peak of the $^rR(9)$ line at a total O_2 pressure of 1330 Pa and temperature of 296 K. The decay in this case is exponential within signal-to-noise limits. However, the decay time constant derived from the fit of a single exponential to the data results in an estimated absorptive peak loss of 8038 ppm/pass. This is ~8% low of the expected peak value of 9251 ppm/pass *(14)*. Peak absorptive losses of 9110 ppm/pass, or only about 1.5% low of the expected value are obtained by using the integral formulation to the observed decays and the measured laser spectrum. Although the agreement with published values is good, the accuracy of these data was limited by several factors common to most CRDS experiments. These include uncertainties in the time-averaged laser bandwidth, variations in the laser/cavity mode detuning, and transverse mode beating in the decay signals. A spectrum of the O_2 $^rR(9)$ line was obtained by determining the losses from a simple exponential fit as the laser was scanned over the transition. This result, given in Figure 2b illustrates that failure to deconvolute bandwidth effects yields a line shape that is broadened relative to the expected nearly Doppler-limited profile.

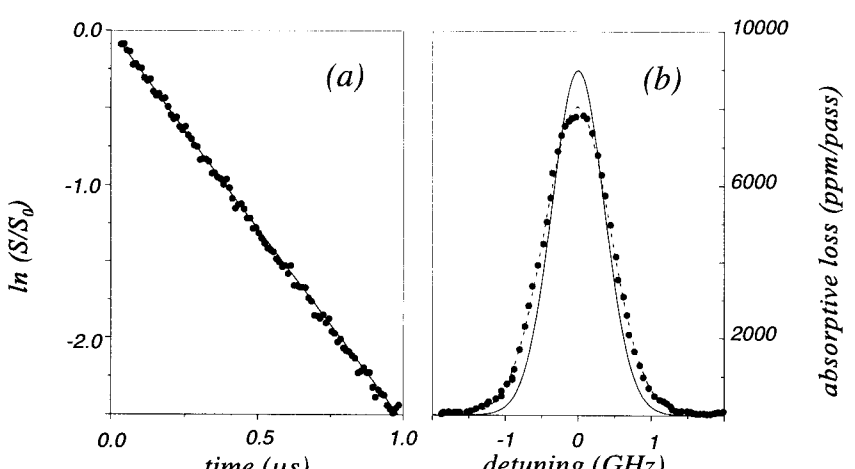

Figure 2: A ringdown signal (a) and rovibronic line profile (b) of the $^rR(9)$ transition of the $^{16}O_2$ A-band measured using a conventional implementation of CRDS.

Measurements Using Short Cavities. To improve on the measurements discussed above, we designed an experimental system to optimize the quantitative measurement capability of CRDS. The approach we chose was predicated on the assumption that the most accurate CRDS measurements would be made with single mode excitation. This also required using a frequency-stabilized laser and a length-stabilized ringdown cavity.

Light for these measurements was generated with an injection-seeded, pulsed optical parametric oscillator (OPO) that was frequency stabilized against a transfer cavity. The resulting frequency stability was estimated to be better than 3 MHz. In seeded operation and when pumped with a fluence of ~2 J/cm^2, the OPO generated ~1 mJ of signal light, in a pulse ~4 ns long with a bandwidth of ~115 MHz. Length stabilization was achieved by constructing a chamber from invar and housing the entire assembly in a temperature regulated enclosure. A pair of 20 cm radius of curvature dielectric mirrors separated by 10.4 cm formed the ringdown cavity. For this setup, $\eta \sim 0.067$. The output mirror was mounted on a tubular piezoelectric element to permit scanning of the ringdown cavity length and hence the cavity resonant frequency. A commercial Si-PIN photodiode package was used to measure the ringdown signals. The amplifier output was terminated into 50 Ω at the input of a 10-bit digital oscilloscope. The electronic bandwidth was 15 MHz. The digitized ringdown decay signals were transferred to a computer and processed on a shot-by-shot basis.

To minimize coupling into higher order transverse modes, the OPO beam was spatially filtered and imaged into the ringdown cavity. About three quarters of the transmitted light could be coupled into TEM_{00}, and no mode with a transverse mode index sum ($m+n$) greater than two was appreciably excited. Ringdown signals from different transverse modes were readily observed and compared. It is interesting to note that the empty cavity ringdown losses were found to increase by ~5 ppm per unit change in the transverse mode index sum. Such large differences cannot be explained by transverse-mode-dependent diffraction losses or the frequency dependence of the mirror reflectivity. These variations perhaps arise from nonidealities in cavity alignment, such as a tilt of the mirror, or nonidealities in the mirrors themselves, such as astigmatism, spatial variations in the surface smoothness, or imperfections in the dielectric stack.

A typical ringdown signal and the associated residuals from a weighted-least-squares fit are shown in Figure 3. This empty cavity signal has a ringdown time of 13.18 μs, corresponding to a mirror loss per pass of 26.33 ppm/pass. The fractional uncertainty in the measured time constant, also extracted from this fit, is 0.03%. A better measure of the uncertainty in the ringdown time is the standard deviation of an ensemble of time constants that is obtained by repeated measurements. It was found that such a distribution typically had a larger standard deviation (0.2-0.4%) than that extracted from a single-shot. This larger number sets the detection limit of this experiment.

To demonstrate the quantitative potential of this ringdown system, the line shape of the $^PP(9)$ rotational transition of^{16} O_2 was measured at a pressure of 1.29 kPa and temperature of 296.0 K. In this experiment, the OPO frequency was scanned in 50 MHz steps, and at each step the OPO and ringdown cavity were brought in to resonance. Ten shots per step were acquired, with each shot processed to yield an average ringdown time, $\bar{\tau}$. At each frequency step, $\bar{\tau}$ and the associated variance in the set of ten measured time constants were calculated. Near the line center, the standard deviation of the ten measured

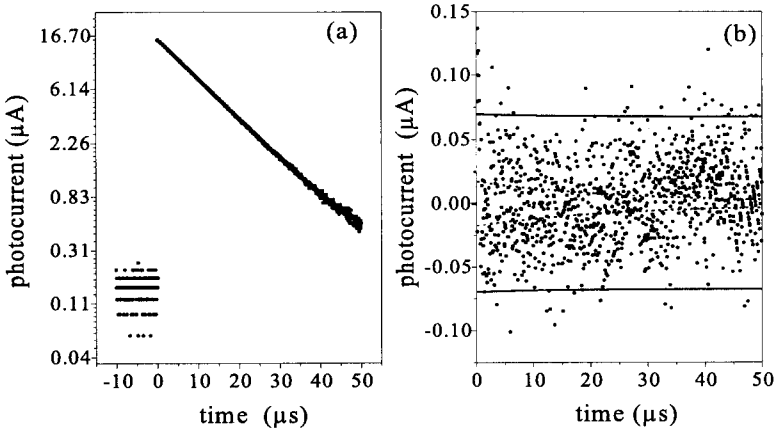

Figure 3: Panel (a) shows a ringdown signal measured using a single mode, pulsed excitation of a short cavity. Panel (b) shows the residuals to a fit of the measured curve. The solid line shows the 2σ uncertainty associated with technical detector noise, and the dashed line is the shot-noise associated with the flux exiting the cavity.

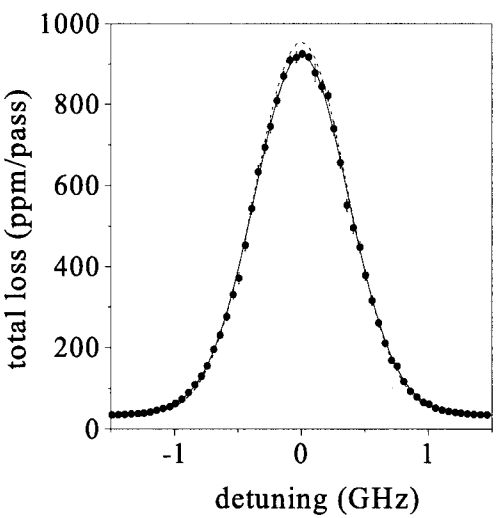

Figure 4: A line profile of the $^{P}P(9)$ transition of th $^{16}O_2$ A-band measured using the short cavity. The 2σ uncertainty at each step is also shown. The solid line is a fit using a Galatry line shape, and the dashed line is a Doppler profile.

time constants increased by a factor of about four compared to the empty cavity, as there are about fifteen times fewer points in the ringdown curves. The results are shown in Figure 4.

These data were fit to two line shape models. First, they were fit using a Galatry line shape and the broadening and narrowing coefficients reported by Ritter and Wilkerson as constants *(14)*. The off-resonance ringdown cavity loss and the transition line strength were varied. For each datum, the weighting coefficient was taken to be the reciprocal of the sum of the measured variance in cavity loss and the variance associated with the uncertainty in the frequency axis, which was estimated to be 10 MHz. Except in the far wings and near the line center, the maximum contribution to the uncertainty in each datum is associated with the imprecision in the frequency axis. This fit gives a line strength of $8.56 \cdot 10^{-24}$ $cm^2\ cm^{-1}$/molecule, about 0.9% larger than that reported by Ritter and Wilkerson. The fit to the line profile is quite good and yields a $\chi^2 = 0.81$. Figure 4 also shows a best-fit Doppler profile. The line strength extracted from this fit is ~0.5% larger than the Ritter and Wilkerson value; however, the quality of this fit is inferior ($\chi^2 = 31$). The discrepancies between the measured profile and best-fit Doppler profile are most notable near line center. The best-fit Doppler profile gave empty-cavity losses of ~34 ppm/pass, ~10% larger than the measured value of 31 ± 0.1 ppm/pass. The ability to distinguish between line shapes demonstrates that the inherent frequency selectivity of optically short cavities can be used to make sensitive and accurate measurements.

Conclusion.

This paper has extended the field-based description of ringdown signals *(5)* to include the case when the cavity is filled with a sample that absorbs in the Beer-Lambert law limit. Expressions for the peak power exiting the cavity, transmitted energy and shot-noise limited absorptivity were derived for the short- and long-cavity limits. It was argued that quantitative absorptivity measurements are best made in the short-cavity limit, and data were presented for both a short- and a conventional, long-cavity implementation of CRDS. The experimental results bolster the conjecture that the most sensitive measurements can be made in the short-cavity case, and also suggest that single mode, pulsed cavity-ringdown spectroscopy can be used for measurements requiring high spectral resolution, such as the measurement of line shapes or saturation spectroscopies.

Literature Cited.

(1) O'Keefe, A.; Deacon, D. A. G. *Rev. Sci. Instrum.* **1988**, *59*, 2544.
(2) Romanini, D.; Lehmann K. K. *J. Chem. Phys.* **1993**, *99*, 6287.
(3) Scherer, J. J.; Paul, J. B.; Collier, C. P.; Saykally, R. J. *J. Chem. Phys.* **1995**, *102*, 5190.
(4) Romanini, D.; Lehmann K. K. *J. Chem. Phys.* **1996**, *105*, 10263.
(5) Hodges, J. T.; Looney, J. P.; van Zee, R. D. *J. Chem. Phys.* **1996**, *105*, 10278.
(6) Zalicki, P.; Zare, R.N. *J. Chem. Phys.* **1995**, *102*, 2708.
(7) Martin, J.; Paldus, B.A.; Zalicki, P.; Wahl, E.H.; Owano, T. G.; Harris Jr., J. S.; Kruger, C.H.; Zare, R. N. *Chem. Phys. Lett.* **1996**, *258*, 63.
(8) Kogelnik, H.; Li, T. *Proc. IEEE* **1966**, *54*, 1312.
(9) Born, M.; Wolf, E. *Principles of Optics;* Pergamon Press: New York, NY, 1980; p 325.

(10) *High-Resolution Spectroscopy;* Shimoda, K., Ed.; Topics in Applied Physics; Springer-Verlag: Heidelberg, Germany, 1976; vol. 13.
(11) Bevington, P. R. *Data Reduction and Error Analysis for the Physical Sciences*, McGraw-Hill: New York, NY, 1969.
(12) Hodges, J. T.; Looney, J. P.; van Zee, R. D. *Appl. Opt.* **1996**, *35*, 4112.
(13) Meijer, G.; Boogaarts, M. G. H.; Jongma, R. T.; Parker, D. H.; Wodtke, A. M. *Chem. Phys. Lett.* **1994**, *217*, 112.
(14) Ritter, K. J.; Wilkerson, T. D. *J. Mol. Spectro.* **1987**, *121*, 1.